Respiratory Syncytial Virus Sequesters NF-κB Subunit p65 to Cytoplasmic Inclusion Bodies To Inhibit Innate Immune Signaling

Fatoumatta Jobe,[a] Jennifer Simpson,[a] Philippa Hawes,[a] Efrain Guzman,[a*] Dalan Bailey[a]

[a]The Pirbright Institute, Guildford, Surrey, United Kingdom

ABSTRACT Viruses routinely employ strategies to prevent the activation of innate immune signaling in infected cells. Respiratory syncytial virus (RSV) is no exception, as it encodes two accessory proteins (NS1 and NS2) which are well established to block interferon signaling. However, RSV-encoded mechanisms for inhibiting NF-κB signaling are less well characterized. In this study, we identified RSV-mediated antagonism of this pathway, independent of the NS1 and NS2 proteins and indeed distinct from other known viral mechanisms of NF-κB inhibition. In both human and bovine RSV-infected cells, we demonstrated that the p65 subunit of NF-κB is rerouted to perinuclear puncta in the cytoplasm, which are synonymous with viral inclusion bodies (IBs), the site for viral RNA replication. Captured p65 was unable to translocate to the nucleus or transactivate a NF-κB reporter following tumor necrosis factor alpha (TNF-α) stimulation, confirming the immune-antagonistic nature of this sequestration. Subsequently, we used correlative light electron microscopy (CLEM) to colocalize the RSV N protein and p65 within bovine RSV (bRSV) IBs, which are granular, membraneless regions of cytoplasm with liquid organelle-like properties. Additional characterization of bRSV IBs indicated that although they are likely formed by liquid-liquid phase separation (LLPS), they have a differential sensitivity to hypotonic shock proportional to their size. Together, these data identify a novel mechanism for viral antagonism of innate immune signaling which relies on sequestration of the NF-κB subunit p65 to a biomolecular condensate—a mechanism conserved across the *Orthopneumovirus* genus and not host-cell specific. More generally, they provide additional evidence that RNA virus IBs are important immunomodulatory complexes within infected cells.

IMPORTANCE Many viruses replicate almost entirely in the cytoplasm of infected cells; however, how these pathogens are able to compartmentalize their life cycle to provide favorable conditions for replication and to avoid the litany of antiviral detection mechanisms in the cytoplasm remains relatively uncharacterized. In this manuscript, we show that bovine respiratory syncytial virus (bRSV), which infects cattle, does this by generating inclusion bodies in the cytoplasm of infected cells. We confirm that both bRSV and human RSV viral RNA replication takes place in these inclusion bodies, likely meaning these organelles are a functionally conserved feature of this group of viruses (the orthopneumoviruses). Importantly, we also showed that these organelles are able to capture important innate immune transcription factors (in this case NF-KB), blocking the normal signaling processes that tell the nucleus the cell is infected, which may help us to understand how these viruses cause disease.

Address correspondence to Dalan Bailey, dalan.bailey@pirbright.ac.uk.

* Present address: Efrain Guzman, Oxford Biomedica (UK) Ltd., Oxford, United Kingdom.

Bovine and human respiratory syncytial virus (bRSV and hRSV, respectively) are closely related viruses that cause acute respiratory illness in cattle and humans, respectively. The viruses infect all ages, but severe illness associated with bronchiolitis and pneumonia is more common in calves (for bRSV) and infants, the elderly, and immunocompromised (for hRSV) (1, 2). Although the process is poorly understood, immune responses to RSV infections are incomplete, leading to reinfection, even in healthy adults (3). In high-risk groups, hRSV infection can be fatal; however, there is no approved vaccine and only a single therapeutic option, namely, monoclonal antibodies against the F protein. While there are available bRSV vaccines, they are mildly protective, and there is evidence for an exacerbation of natural infection (4). Both viruses were recently taxonomically reclassified as species *Bovine* and *Human orthopneumovirus* within the *Orthopneumovirus* genus of the *Pneumoviridae* family (5).

bRSV and hRSV are enveloped viruses with a single-stranded negative-sense RNA genome, ~15 kb long, which encodes 11 proteins from 10 mRNAs. Although bRSV and hRSV are restricted to their individual hosts, the viruses and the diseases they cause are similar, making bRSV an excellent model for studying hRSV-host interactions. Virus infection and replication within the cell trigger pattern recognition receptors (PRRs), such as Toll-like receptors (TLRs) and cytoplasmic nucleic acid receptors (RIG-I and MDA5), which in turn induce NF-κB- and IRF-dependent signaling (6–8). NF-κB and IRF are two families of transcription factors that exist as homo- or heterodimers, and their activation is regulated at multiple levels. For example, NF-κB p65/p50 dimers are sequestered in the cytoplasm bound to the inhibitor IκBα (9, 10). Phosphorylation of IκBα by the IκB kinase (IKK) complex targets it for proteasomal degradation releasing p65/p50 for phosphorylation and translocation into the nucleus. Activation and nuclear translocation of IRF-3 homodimers also depend on phosphorylation, through the kinases TBK1/IKKε (11). Upon activation, these critical transcription factors regulate host cell innate responses, e.g., by inducing cytokines with antiviral activity, including type 1 interferons (IFNs), tumor necrosis factor alpha (TNF-α), and interleukin-1 (IL-1). Importantly, the mechanisms by which RSV induce or inhibit these signaling pathways are not fully understood.

To overcome this ubiquitous first line of defense, viruses have evolved various inhibitors to modulate these pathways. Viral immune evasion mechanisms include the targeting of receptors, adaptor proteins, and/or intracellular kinases in the signaling pathways described above or indeed directly targeting the transcription factors and their regulators (12, 13); and in this regard, RSV is no exception. The RSV SH protein has been shown to be involved in inhibiting NF-κB activation (14, 15), although the exact mechanism of this antagonism is yet to be characterized. As an alternative strategy the RSV NS1 and NS2 proteins have been shown to antagonize IFN-mediated host responses by targeting both type I and III IFN induction (16–18) and signaling (19). In addition, NS2 interacts with RIG-I inhibiting its interaction with the mitochondrial antiviral-signaling protein (MAVS) (20). Similarly, NS1 can inhibit phosphorylation of IRF-3 by interacting with MAVS (21). Recently, the NS proteins have also been shown to be involved in the formation of an "NS-degradasome" that promotes the degradation of components of IFN induction or signaling, including RIG-I, IRF-3, IRF-7, TBK1, and STAT2 (22). Consequently, activation of the cytotoxic T lymphocyte component of the adaptive immune response is also suppressed (23). hRSV has also been shown to employ an additional mechanism of innate immune antagonism whereby MAVS and MDA5 are sequestered into inclusion bodies (IBs), likely through interaction with the RSV nucleoprotein (N protein) (24). Other cellular proteins involved in the cellular response to viral infection, such as p38 mitogen-activated protein kinase (MAPK) and O-linked N-acetylglucosamine transferase (OGT), have also been shown to be recruited into IBs (25).

The cytoplasmic inclusion bodies induced by hRSV infection share many characteristics with liquid organelles or biomolecular condensates (24–26) having similarity to stress granules, P-bodies, and nucleoli. They are also structurally and functionally similar to viral inclusions formed by rabies, human metapneumovirus, and measles viruses

(27–30) and likely represent an essential component of the life cycle of many negative-sense RNA viruses. The term inclusion bodies is actually quite misleading since this phrase is also widely used in biology to describe misfolded recombinant protein or aggregates. For viral IBs from negative-sense RNA viruses, it will be useful moving forward to either rename these structures or alternatively to define them based on the presence of an identifiable marker. For the pneumoviruses, these membraneless organelles have been shown to contain N, P, L, and M2-1 (26, 29–31), which are viral proteins involved in viral genome replication and mRNA transcription, together with the M protein. The nucleocapsid protein likely represents the most appropriate marker, and therefore, throughout the manuscript when we refer to RSV IBs, we are referring to N-positive inclusions with properties of a biomolecular condensate. Importantly, the presence of viral genomic RNA and mRNA within the IB strongly suggests that these organelles are functional and are the primary site for viral RNA replication within the infected cell (26), although this does not appear to be universal a trend since viral RNA replication of Nipah virus (NiV) was recently shown to occur outside both its structurally distinct IB populations (32). For RSV and related viruses, ectopic coexpression of the N and P proteins alone results in the formation of IB-like structures, indicating a evolutionarily conserved mechanism for IB formation (24, 26, 28, 30, 31). Collectively, these data provide strong evidence that events in the bRSV life cycle are not randomly distributed throughout the cell cytoplasm; instead, components of the viral genome, replication machinery, and its intermediates are likely to be sequestered, away from innate immune sensors, in intracellular compartments which are *de facto* viral replication complexes. However, to date there is no evidence on the formation of IBs in bRSV-infected cells nor, more broadly, any detailed characterization of the immunomodulatory effects of the RSV IB on two integral innate immunity transcription factors, namely, NF-κB and IRF3.

Here, we show that in both hRSV- and bRSV-infected cells, the NF-κB subunit p65 is rapidly sequestered into perinuclear intracytoplasmic puncta. Consequently, activation and nuclear translocation of sequestered NF-κB p65 in response to virus infection and TNF-α stimulation are both inhibited. Using both immunofluorescence confocal microscopy and correlative light electron microscopy (CLEM), these puncta were found to be synonymous with the RSV inclusion bodies induced by virus infection. Transmission electron microscopy confirmed that bRSV IBs are not membrane bound but instead are liquid organelles, likely formed following liquid-liquid phase separation (LLPS). Interestingly, IBs formed by ectopic N and P coexpression were also proficient in colocalizing p65. In addition, p65 recruitment was not host-range specific, with both human and bovine RSV being capable of sequestering p65, regardless of host cell origin. In addition, we present the first detailed evidence of IB formation in bRSV-infected cells, confirming that these viral organelles are the sites of viral RNA replication. Taken together, our data show an evolutionarily conserved mechanism by which RSV IBs function to compartmentalize viral replication and actively antagonize the innate immune response to infection.

RESULTS

bRSV infection induces IRF3, but not NF-κB, nuclear translocation. Given the established role of NF-κB and IRF3 signaling pathways in the cell's innate response and clearance of viral infection, we used multiple approaches to examine the activation of these transcription factors following bRSV infection. Vero cells were infected with bRSV at a multiplicity of infection (MOI) of 1 for 24 h. Cells were then immunostained for bRSV F as a marker for infection as well as for the NF-κB subunit p65 or, separately, IRF3. Immunofluorescence (IF) analysis of mock-infected cells confirmed that both transcription factors are normally located in the cytoplasm (Fig. 1A). When the NF-κB and IRF3 pathways were stimulated in mock-infected cells with agonist treatment [human TNF-α (hTNF-α) and poly(I:C), respectively], both the NF-κB subunit p65 and IRF3 translocated from the cytoplasm to the nucleus, as expected (Fig. 1A, top, inset zooms). However, although infection with bRSV induced similar levels of IRF3 nuclear translocation
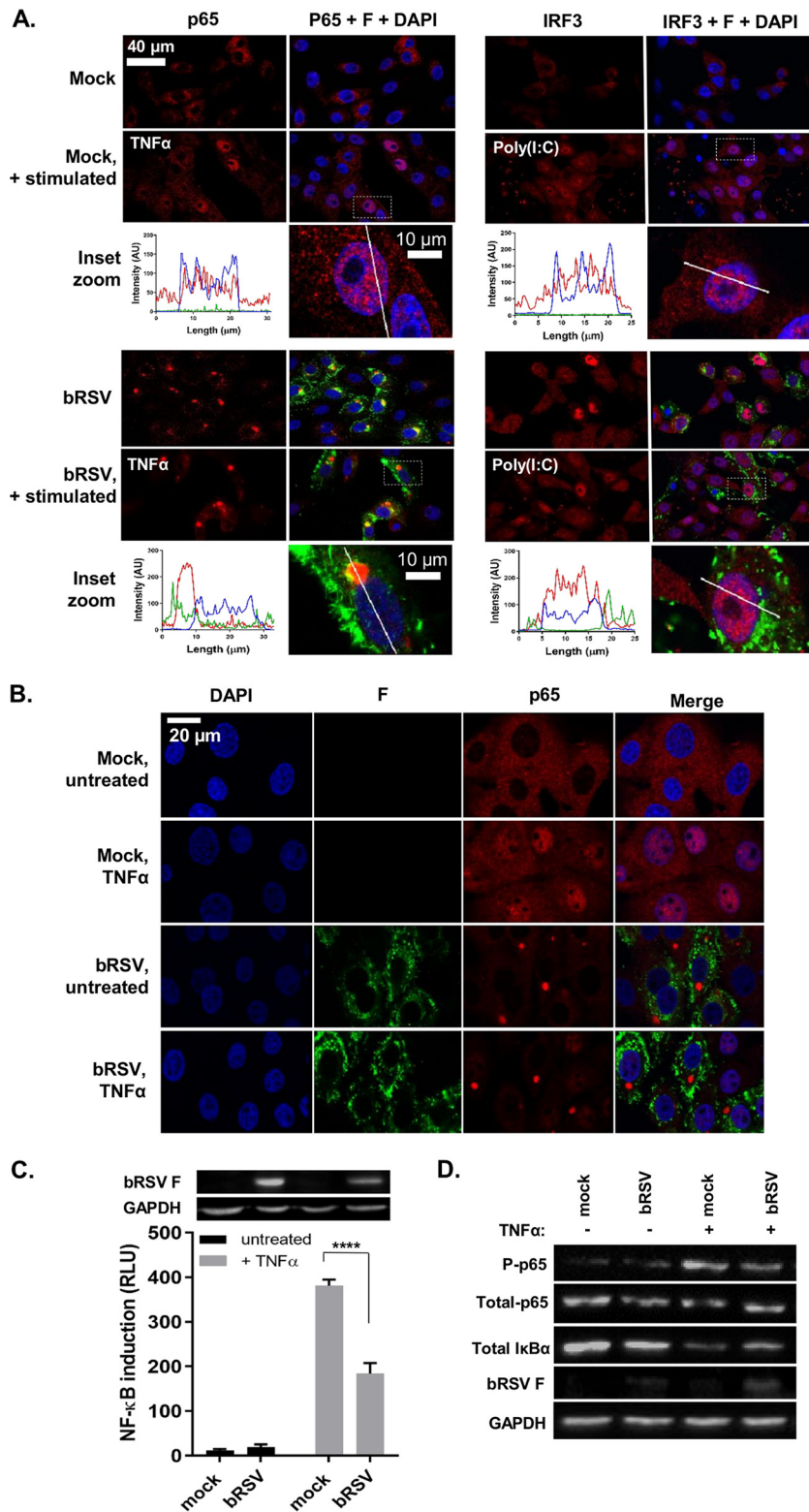
FIG 1 bRSV infection induces IRF3, but not NF-κB, nuclear translocation. (A) Vero cells uninfected (mock) or infected with bRSV at an MOI of 1 for 24 h were left untreated, stimulated with 20 ng/ml hTNF-α for 30 min, or transfected with 2.5 μg/ml poly(I:C) and incubated for 6 h at 37°C. Cells were then fixed and immunostained with anti-RSV F (green) and anti-NF-κB p65 or anti-IRF3 (red) antibodies. Cell nuclei were stained with DAPI (blue) and images obtained using a Leica TCS SP5 confocal microscope. The boxed areas are shown magnified in the panels below (inset zoom). Graphs show fluorescent line intensity profiles along the respective white lines within these inset zooms. (B) NF-κB activation in bRSV-infected MDBK cells. MDBK cells mock infected or infected with bRSV at an MOI of 1 for 24 h were left untreated

(Continued on next page)

(Fig. 1A, bottom right), significantly, the NF-κB subunit p65 remained cytoplasmic, coalescing into intracytoplasmic puncta, mostly perinuclear, and present only in infected cells (Fig. 1A, bottom left). Fluorophore intensity profile analysis was then performed to assess the relative accumulation of both p65 and IRF3 in infected and/or stimulated cells. For IRF3, poly(I:C) stimulation of infected cells enhanced its nuclear translocation, relative to uninfected cells (Fig. 1A, bottom right, inset zoom). However, IF and intensity profile analysis revealed that, even in the case of hTNF-α stimulation, p65 nuclear translocation in bRSV-infected cells was absent and that most p65 remained in the observed perinuclear puncta (Fig. 1A, bottom left, inset zoom). bRSV can infect a broad range of host cells in vitro—growing to similar titers in both Vero and Madin-Darby bovine kidney (MDBK) cells (data not shown). To examine the apparent innate immune antagonism in bovine cells, equivalent infections were performed in MDBK cells. These experiments confirmed the same p65 sequestration into perinuclear puncta following bRSV infection, as well as the related insensitivity to TNF-α stimulation (Fig. 1B), indicating a conserved mechanism of antagonism active in both primate and ruminant cells.

To examine the effect of this sequestration on NF-κB signaling, we next employed a luciferase reporter assay to assess NF-κB transactivation. HEK293T cells were infected with bRSV at an MOI of 1, before being transfected with the NF-κB reporter and subsequently treated with or without TNF-α (Fig. 1C). Interestingly, infection without TNF-α treatment did not result in any significant activation of the reporter, despite demonstrable viral protein production (Fig. 1C, black bars and RSV F Western blot), indicating that even in the presence of active viral replication there is little to no activation of the NF-κB signaling pathway in bRSV-infected cells. Indeed, activation of the NF-κB reporter was seen only following the addition of 20 ng/ml of exogenous hTNF-α; however, this activation was significantly less in infected cells than in the mock cells (Fig. 1C, gray bars). Separately, we also examined protein levels of p65 (total and transiently phosphorylated) and IκBα, components of NF-κB signal transduction, in infected Vero cells with and without TNF-α stimulation. As expected, TNF-α treatment of mock-infected cells resulted in an increase in p65 phosphorylation and a decrease in total IκBα (presumably the result of proteasomal degradation following its own phosphorylation) (Fig. 1D, mock −/+ TNF-α) (9). The detected levels of phospho-NF-κB p65 and total IκBα in infected cells (Fig. 1D, infected −/+ TNF-α) confirmed the lack of activation during infection and also the modest NF-κB activation induced by bRSV infection with subsequent TNF-α treatment observed in Fig. 1C. Together, the data strongly suggest that NF-κB signaling is inhibited by bRSV infection due to its sequestration into intracytoplasmic puncta. Importantly, these data also indicate that the sequestered p65 is not in a transcriptionally active state since infection did not result in a marked increase in p65 phosphorylation or demonstrable IκBα degradation.

bRSV replication induces the recruitment of the NF-κB subunit p65 into intracytoplasmic bodies distinct from stress granules. NF-κB p65 puncta were only observed in bRSV-infected cells showing detectable levels of F protein, indicating a correlation between productive infection and sequestration (Fig. 1A). To examine this

FIG 1 Legend (Continued)

or stimulated with 20 ng/ml hTNF-α for 30 min. Cells were then fixed and immunostained with anti-RSV F (green) or anti-NF-κB p65 (red) antibodies. Cell nuclei were stained with DAPI (blue) and images obtained using a Leica TCS SP5 confocal microscope. (C) 293T cells were mock infected or infected with bRSV at an MOI of 1. At 6 h p.i., cells were transfected with 100-ng NF-κB FLuc reporter and 10-ng TK-renilla luciferase and incubated at 37°C. At 18 h posttreatment (p.t.), cells were left untreated or stimulated for 16 h with 20 ng/ml hTNF-α. Cells were then lysed and analyzed for firefly and renilla luciferase activities. Graph depicts means ± SD of three replicates from the same experiment. As controls, the levels of RSV F and glyceraldehyde-3-phosphate dehydrogenase (GAPDH) were analyzed by Western blotting on a fourth replicate. Statistical significance determined by ANOVA as described in the Materials and Methods; ****, $P < 0.0001$. (D) Vero cells mock infected or infected with bRSV at an MOI of 2 for 24 h were left untreated or stimulated with 20 ng/ml hTNF-α for 10 min. Cells were then lysed and analyzed by Western blotting for phosphorylation of p65 using phospho-specific forms of the antibody, total p65, IκBα, and RSV F. GAPDH was detected as a loading control.
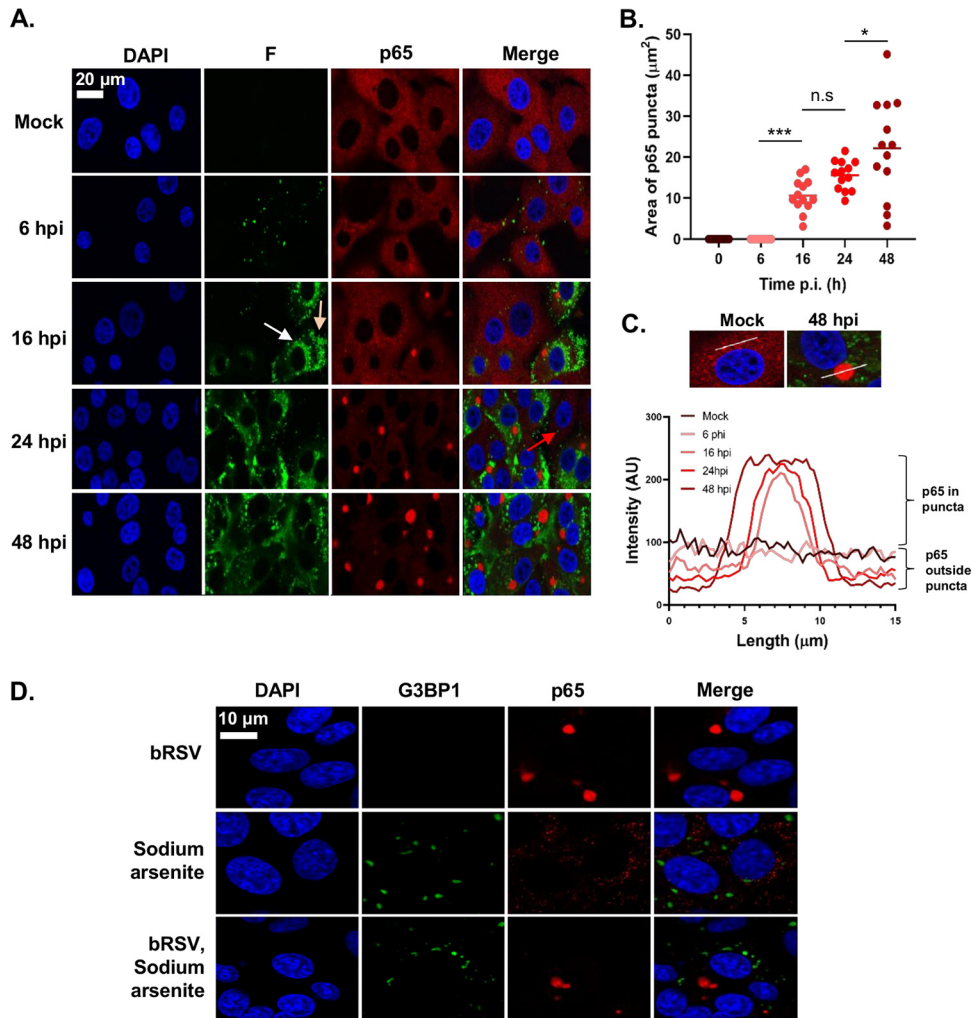
FIG 2 BRSV replication induces the recruitment of the NF-κB subunit p65 into intracytoplasmic bodies distinct from stress granules. (A) MDBK cells were mock infected or infected with bRSV. At the indicated times p.i. cells were fixed and immunostained with anti-RSV F (green) and anti-NF-κB p65 (red) antibodies. Nuclei were stained with DAPI (blue) and images obtained using a Leica TCS SP5 confocal microscope. (B and C) Quantification of p65 puncta in A obtained using the quantify tool of Leica LAS AF Lite software as described in the Materials and Methods. (B) Surface area of 13 p65 puncta per time point and mean area are indicated. Statistical significance determined by ANOVA as described in the Materials and Methods; n.s, nonsignificant; *, $P < 0.05$; ***, $P < 0.001$. (C) Graph showing the line intensity profiles along chosen 15-μm lines of interest (example micrographs: 15 μm drawn across a puncta or across the cytoplasm in mock cells) of an average of five puncta per time point. (D) Vero cells were infected with bRSV or mock infected. At 24 h p.i., cells were treated with 500 μM sodium arsenite or mock treated for 1 h. Cells were then fixed and immunostained with anti-G3BP1 (green) and anti-NF-κB p65 (red) antibodies. Nuclei were stained with DAPI (blue) and images obtained using a Leica TCS SP5 confocal microscope.

correlation and define the kinetics of p65 sequestration over time, MDBK cells were infected at an MOI of 1 and fixed at different times postinfection (p.i.), before being permeabilized and before the distribution of p65 and RSV F was analyzed by IF. Detectable NF-κB p65 puncta (>3 μm²) were apparent in infected cells by 16 h p.i. (Fig. 2B), correlating with significant levels of F expression (Fig. 2A). Interestingly, two populations of F protein were present at this stage, a perinuclear, presumably endoplasmic reticulum (ER)- or vesicle-associated population (Fig. 2A, white arrow) and a peripheral more filamentous-like population, possibly the site of virion biogenesis (Fig. 2A, beige arrow)—neither of which appeared to colocalize in any significant way with p65. By 24 h p.i., all infected cells contained at least one p65 punctum, with none being observed in nearby uninfected cells (Fig. 2A, red arrow). Using fluorophore line of interest analysis, we were also able to assess the ratio of cytoplasmic- to punctum-

localized p65 as well as the increasing diameter of these aggregates. As infection proceeded, the intensity of p65 in the puncta increased as the level of disperse p65 in the cytoplasm decreased (Fig. 2C, "p65 in puncta" versus "p65 outside puncta"), indicating coalescence and supporting our observations in Fig. 1D that the total amount of p65 in cells does not dramatically change during infection, only its subcellular localization. Average punctum size increased as infection progressed, with p65 aggregations at 48 h p.i. having a mean area of 22.18 μm^2 (Fig. 2B). Smaller p65 puncta ($<$10 μm^2) were also observed at 48 h p.i., most likely the result of nascent infections in nearby cells. By this time, F protein expression was markedly different, with less distinct populations of protein; however, there was still no obvious colocalization with the p65 puncta. A similar pattern of results was also observed in Vero cells (data not shown).

Our first line of inquiry following the identification of p65 puncta in bRSV-infected cells was based on their visual similarity to protein and mRNA aggregations that form in cells in response to cellular stress and viral infections, so-called stress granules (SGs). A wide range of viruses have been shown to either induce or inhibit SG formation to their advantage (33); however, there are contradictory findings on SG induction by RSV (25, 34–36). To examine the potential relationship between these p65 puncta and SG, we induced SG formation in bRSV-infected cells with sodium arsenite treatment and performed coimmunostaining for p65 and G3BP1 (an SG marker) in fixed cells. Although we were able to successfully stimulate the production of SGs in Vero cells, our analysis showed that the p65 puncta were entirely distinct from these granules (Fig. 2D). Tangentially, this experiment also demonstrated that bRSV infection does not significantly induce SG formation.

The NF-κB subunit p65 colocalizes with viral inclusion bodies independently of RSV-encoded immunomodulators. RSV has a relatively small genome, encoding 11 proteins from 10 genes (Fig. 3A). Recent work has demonstrated that hRSV infection induces the formation of inclusion bodies (IBs) which contain components of the RNA polymerase complex and ribonucleoprotein (RNP), notably N and P (26); however, to our knowledge, similar IBs have not been identified, or functionally characterized, in bRSV-infected cells. To examine the presence of IBs, the distribution of bRSV proteins, and, collectively, their subcellular localization in relation to the observed p65 puncta, we infected Vero cells and fixed them, along with mock-infected cells, for IF analysis at 24 h p.i. These cells were then coimmunostained for p65 and bRSV N, P, M, or F proteins. As expected, neither p65 puncta nor bRSV proteins were detected in mock-infected cells (Fig. 3B). Similarly, as described in Fig. 1 and 2, RSV F did not colocalize with p65 or show evidence of subcellular localization with IB-like structures. In contrast, in infected cells, three of the viral proteins (N, P, and M) predominately localized to large intracytoplasmic organelles, characteristic of viral inclusion bodies (Fig. 3B, green panels), although smaller, spherical N-positive IBs were also present (see below). Although there was a various degree of cytoplasmic signal for N, P, and M outside the IBs, most of the IF signal was found within these structures (Fig. 3B, zoomed inset and line of interest plots). The sub-IB localization of bRSV N and P was similar to that previously described for hRSV, with N and P being found on the periphery of the organelle (26). The significant intra-IB localization of the M protein at 24 h p.i., as well as its partial nuclear localization, is consistent with previously reported IF in RSV-infected cells (37, 38). However, the role of M in RNA virus IBs reflects an interesting point of divergence; with some viral IBs being M positive (e.g., RSV) and others negative (e.g., rabies) (39). Significantly, the larger N-, P-, or M-positive IBs were, in the majority of cases, also p65 positive (Fig. 3B, red IF panels) identifying, for the first time, that this NF-κB component was being recruited to RSV inclusion bodies in infected cells. To examine this in detail, we next characterized the number, size, and p65 status of N-positive IBs in infected cells, observing that they were numerous and mostly localized in the median section of the cell. We therefore obtained images from multiple planes in this section to assemble max intensity z-stacks to aid quantification. From 16 h p.i., N- and p65-positive IBs were evident throughout the cell in a conserved pattern
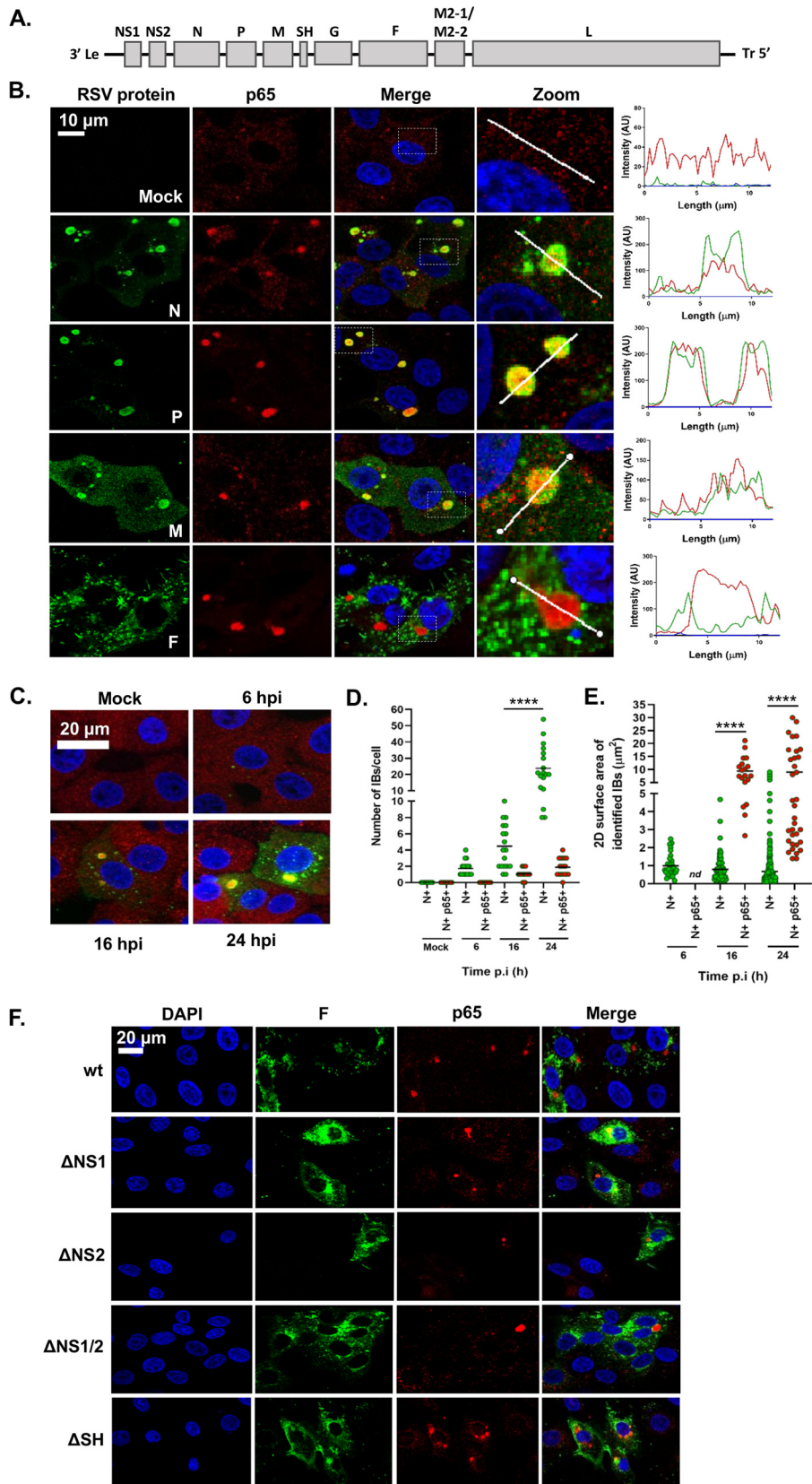
FIG 3 The NF-κB subunit p65 colocalizes with viral inclusion bodies independently of RSV-encoded immunomodulators. (A) Schematic depiction of the bRSV genome showing organization of the encoded genes. (B) Vero cells, mock infected or infected with bRSV for 24 h, were fixed and immunostained with

(Continued on next page)

consisting of a single, large, and perinuclear IB with multiple smaller inclusions more evenly distributed through the cytoplasm (Fig. 3C; see Videos S1 and S2 in the supplemental material). Using z-stacks, we quantified the number per cell (counting 18 cells per sample, per time point) and surface area of N- and/or p65-positive structures of >0.1 μm^2, observing them both increasing as infection progressed. The average number of IBs of >0.1 μm^2 grew from 1.7 per cell at 6 h p.i. to 23.8 at 24 h p.i. (Fig. 3D). Their mean area also increased to 8.99 μm^2 by 24 h p.i. (Fig. 3E), significantly influenced by the presence and growth of the larger IB. p65-positive IBs were detected from 16 h p.i.; however, p65 was only detected in larger IBs (>1.39 μm^2) (Fig. 3E) with up to 4 of them being evident per cell (Fig. 3D). In conclusion, although multiple N-positive IBs are present in infected cells, it is predominantly the larger IBs which contain the sequestered p65. Together, these data suggest that bRSV infection induces the formation of IBs in the cytoplasm of infected cells, which are organelles also involved in sequestering cellular proteins to effect immunomodulation. To our knowledge, this represents an entirely novel mechanism of viral inhibition of NF-κB signaling since it is the sequestration of signaling components to a viral organelle, rather than the degradation commonly seen (12, 22), which leads to the innate immune antagonism described in Fig. 1.

We next examined whether the established bRSV-encoded immunomodulatory proteins NS1, NS2 (18), and SH (14, 15) are responsible for this p65 sequestration. We infected cells with wild-type (wt) bRSV or recombinant bRSVs which do not express these proteins (ΔNS1, ΔNS2, ΔNS1/2 [a double knockout], or ΔSH) (15, 40). IF analysis of these samples identified p65 puncta in all infected cells (Fig. 3F), suggesting that these bRSV-encoded immunoantagonists do not play a significant role in either the formation of IBs or the sequestration of p65 to these structures.

bRSV IBs are sites of RNA replication, but p65 does not specifically colocalize with M2-1 or nascent viral RNA in IBAGs. hRSV inclusion bodies have previously been shown to be the sites of virus transcription and replication (25, 26, 41). To confirm bRSV IBs are also the site of viral RNA replication, we carried out nascent RNA labeling using 5-ethynyl-uridine (5EU) incorporation. Mock-infected MDBK cells, incubated with 5EU for 1 h, revealed, as expected, 5EU incorporation into cellular RNA in the nucleus (Fig. 4A, top row). When cellular transcription was inhibited following preincubation of mock-infected cells with actinomycin D (Act D) for 1 h, this signal was lost. 5EU labeling performed on bRSV-infected cells without Act D treatment did not reveal significant evidence for viral replication in IBs, perhaps due to overrepresentation of cellular RNA synthesis. However, in the presence of Act D, labeled, newly synthesized RNA could only be seen in the N-positive IBs, presumably the result of viral replication. This colocalization of 5EU incorporation and N protein within IBs provides strong evidence that bRSV IBs are the sites of viral RNA replication. A more detailed look at the IBs (Fig. 4A, inset zoom and line of interest plot—asterisks) revealed partial sub-IB organization to the RNA within these structures. Interestingly, a recent study on hRSV IBs identified similar functional compartments within IBs termed inclusion body-associated granules (IBAGs) (26). They were shown to concentrate newly synthesized viral mRNA and the

FIG 3 Legend (Continued)
rabbit anti-NF-κB p65 (red) and mouse monoclonal anti-RSV N, P, M, or F antibodies (green). Nuclei were stained with DAPI (blue) and images obtained using a Leica TCS SP5 confocal microscope. Zoom panel shows magnification of IBs boxed in the merge panel. Graphs shows fluorescent intensity profiles along the indicated white lines drawn across one or two IBs. (C) MDBK cells were mock infected or infected with bRSV. At the indicated times p.i., cells were fixed and immunostained with anti-RSV N (green) and anti-NF-κB p65 (red) antibodies. Images are max intensity Z-stacks of 8 planes 0.5 μm apart. Cytoplasmic bodies (area, >0.1 μm^2) from the Z-stacks were quantified in a total of 18 infected cells per time point as detailed in the Materials and Methods. (D) Number of N- and N- and p65-positive bodies per cell at the indicated time points. (E) Surface area of identified N- and N- and p65-positive IBs. Statistical significance determined by ANOVA as described in the Materials and Methods; ****, $P < 0.0001$. (F) Vero cells were infected with wt bRSV, ΔNS1, ΔNS2, ΔNS1ΔNS2, or ΔSH bRSV. At 24 h p.i., cells were fixed and immunostained with rabbit anti-NF-κB p65 (red) and mouse anti-RSV F (green) antibodies. Cell nuclei were stained with DAPI (blue) and images obtained using a Leica TCS SP5 confocal microscope.
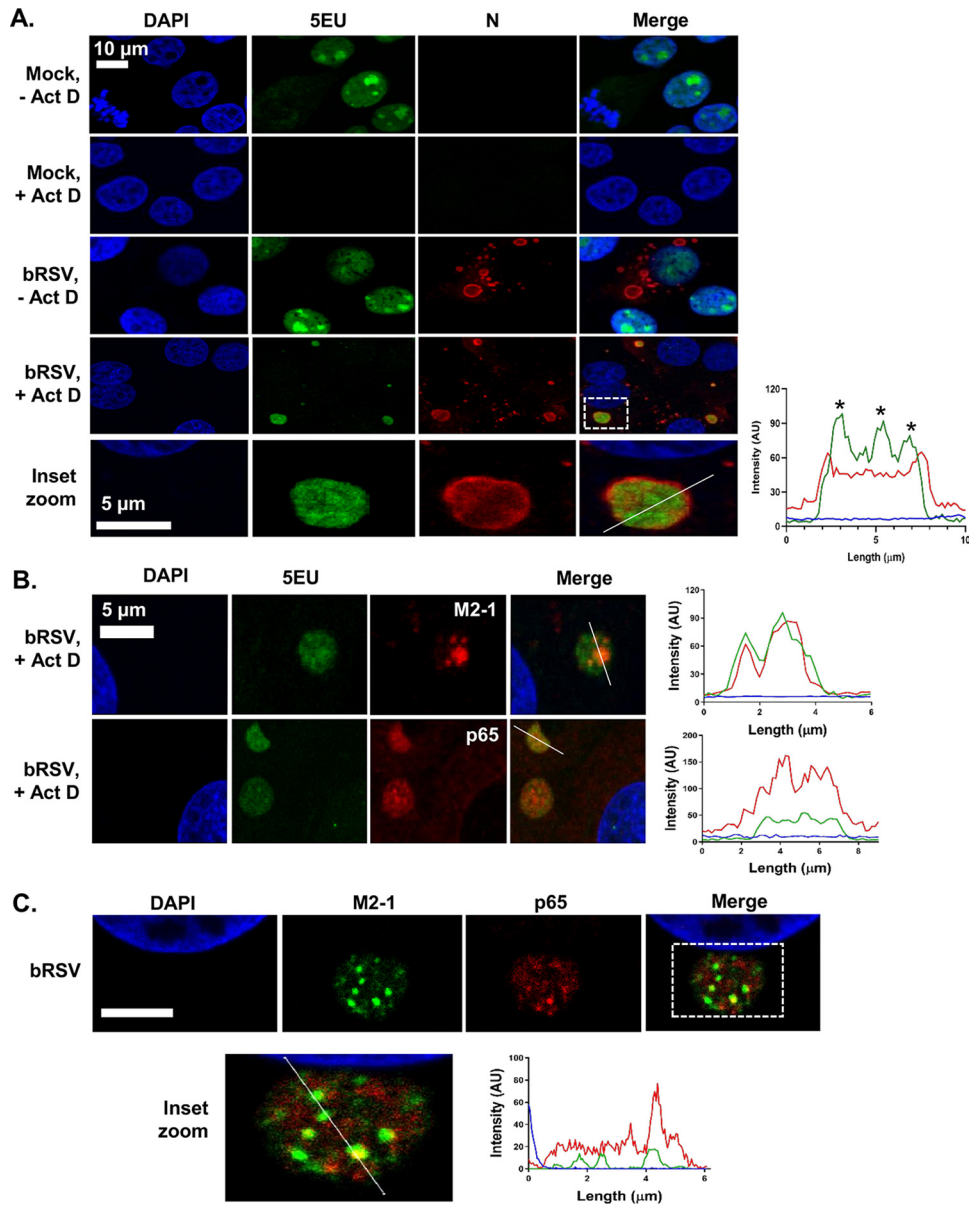
FIG 4 bRSV IBs are sites of RNA replication, but p65 does not specifically colocalize with M2-1 or nascent viral RNA in IB-associated granules (IBAGs). **(A** and **B)** MDBK cells were mock infected or infected with bRSV. After 24 h, cells were incubated with vehicle or 20 μg/ml actinomycin D (Act D) for 1 h to inhibit cellular transcription. 5-Ethynyl uridine (5EU) was then added for another 1 h and the cells fixed. 5EU incorporated into newly synthesized RNA was detected using Alexa Fluor 488-azide (green) as described in the Materials and Methods. Cells were then immunostained with anti-RSV N, M2-1, or anti-NF-κB p65 antibodies (red). Cell nuclei were stained with DAPI (blue) and images obtained using a Leica TCS SP5 confocal microscope. Bottom of A (inset zoom) shows the boxed area (in merge of bRSV, +Act D) magnified. Graphs show fluorescent intensity profiles along the indicated white lines drawn across the IBs. Asterisks in A indicate areas of increased 5EU staining within the IB. (C) Vero cells infected with bRSV for 24 h were fixed and immunostained with rabbit anti-NF-κB p65 (red) and mouse anti-M2-1 (green) antibodies. Cell nuclei were stained with DAPI (blue) and images obtained using a Leica TCS SP5 confocal microscope. Bottom image shows a higher magnification of the boxed area; scale bar corresponds to 4 μm. Graphs show fluorescent intensity profiles along the indicated white line.

viral M2-1 protein but not genomic RNA or the N, P, and L proteins. To confirm the presence of IBAGs in bRSV IBs, we immunostained bRSV-infected cells for M2-1 following nascent viral RNA labeling, observing colocalization of both these components (Fig. 4B). The intra-IB organization of RNA replication and M2-1 protein into IBAGs appears, therefore, to be a structurally conserved aspect of orthopneumovirus IBs. We next examined the potential colocalization of p65 with these sites of nascent viral RNA

(vRNA) localization (IBAGs). Although we observed partial sub-IB localization signals for p65, this did not always colocalize with vRNA (Fig. 4B) or, in subsequent experiments, M2-1 (Fig. 4C). These findings suggest that there are multiple subcompartments within bRSV IBs, in addition to IBAGs, which potentially carry out a distinct range of functions.

bRSV IBs are membraneless liquid organelles. IBs and IB-like structures form by liquid-liquid phase separation (LLPS) which favors macromolecule-macromolecule over macromolecule-water interactions (42–44). The resulting biomolecular condensates are not surrounded or compartmentalized by a membrane, distinguishing them from many other organelles found in the cytoplasm (44, 45). To examine the ultrastructural properties of the bRSV IBs, we first performed standard transmission electron microscopy (TEM) of infected cells. Vero cells were infected with bRSV at an MOI of 1 and fixed for TEM analysis at 24 and 48 h p.i. Granular structures with high electron density, characteristic of RNA virus inclusion bodies, were identified at both time points, often in close proximity to the nucleus (Fig. 5A). Smaller structures (1 to 2 μm in diameter) were predominantly rounder in nature than their larger (>3 μm in diameter), more pleomorphic counterparts (Fig. 5A). As expected, these structures were not membrane bound or directly associated with subcellular organelles; however, rough endoplasmic reticulum (RER) and mitochondria were frequently found in close proximity (Fig. 5A). These structures are similar to those previously reported for other RNA viruses (28, 39), supporting our conclusion that bRSV also forms membraneless IBs in infected cells.

Various reports have also demonstrated that IBs can rapidly change their size due to fusion or fission while remaining spherical in nature, a characteristic feature of these liquid organelles (42). Rabies virus inclusion bodies, termed negri bodies, have been shown to rapidly dissolve and reform in response to hypotonic shock, demonstrating the dynamic nature of these structures (27, 28, 46). To assess the sensitivity of bRSV IBs to hypotonic shock, Vero cells, infected with bRSV for 24 h, were incubated with Dulbecco's modified Eagle's medium (DMEM; diluted to 20% in H_2O) for 20 min. Cells were then fixed and immunostained for the N protein. Many of the smaller spherical IBs showed evidence of dissolution following hypotonic shock (Fig. 5B, iv); however, unlike rabies virus negri bodies, the larger bRSV IBs remained intact following this significant period of cellular osmotic shock (Fig. 5B, iii). Of note, incubation beyond 20 min was not possible because of the associated cytotoxicity. In addition, a large percentage of the sequestered p65 in these larger IBs remained tightly associated with the intact structure (Fig. 5C). Recently, Zhou et al., demonstrated that larger measles IBs had lower rates of fluorescence recovery after photobleaching (FRAP) than that of their smaller counterparts, postulating that these structures had acquired a more gel-like property. The acquisition of this gel-like status, which is also less likely to exchange molecules with the surrounding cytoplasm, has been linked to aging of phase-separated organelles—a continuum which ends with the formation of irreversible aggregates (47). The insensitivity of large bRSV IBs to osmotic shock, and the maintenance of p65 within the IB even under these harsh conditions, is perhaps the result of them acquiring gel-like status, a property which may be linked to the age and size of individual IBs within infected cells.

Finally, to examine the sub-IB localization of RSV N and p65 in relation to our ultrastructural analysis of IBs, we performed correlative light electron microscopy (CLEM). Vero cells were infected at an MOI of 1 and analyzed at 24 and 48 h p.i., first by confocal microscopy using N and p65 antibodies to immunolabel these proteins (Fig. 5D). The same cells, identified by grid reference, were then isolated, embedded, and sectioned with their ultrastructure subsequently analyzed by TEM. Importantly, these CLEM data confirmed that the electron dense granular structures seen by TEM (Fig. 5A) are synonymous with the N, P, M, and p65 stained IBs seen in IF microscopy (Fig. 3B). To our knowledge, this is the first CLEM to be performed on an RNA virus IB. An overlay of the two images confirmed that bRSV IBs had retained the electron-dense granular structure characteristic of liquid organelles, even with the chemical permeabilization required for IF antibody labeling (Fig. 5C). Our CLEM data also confirmed the
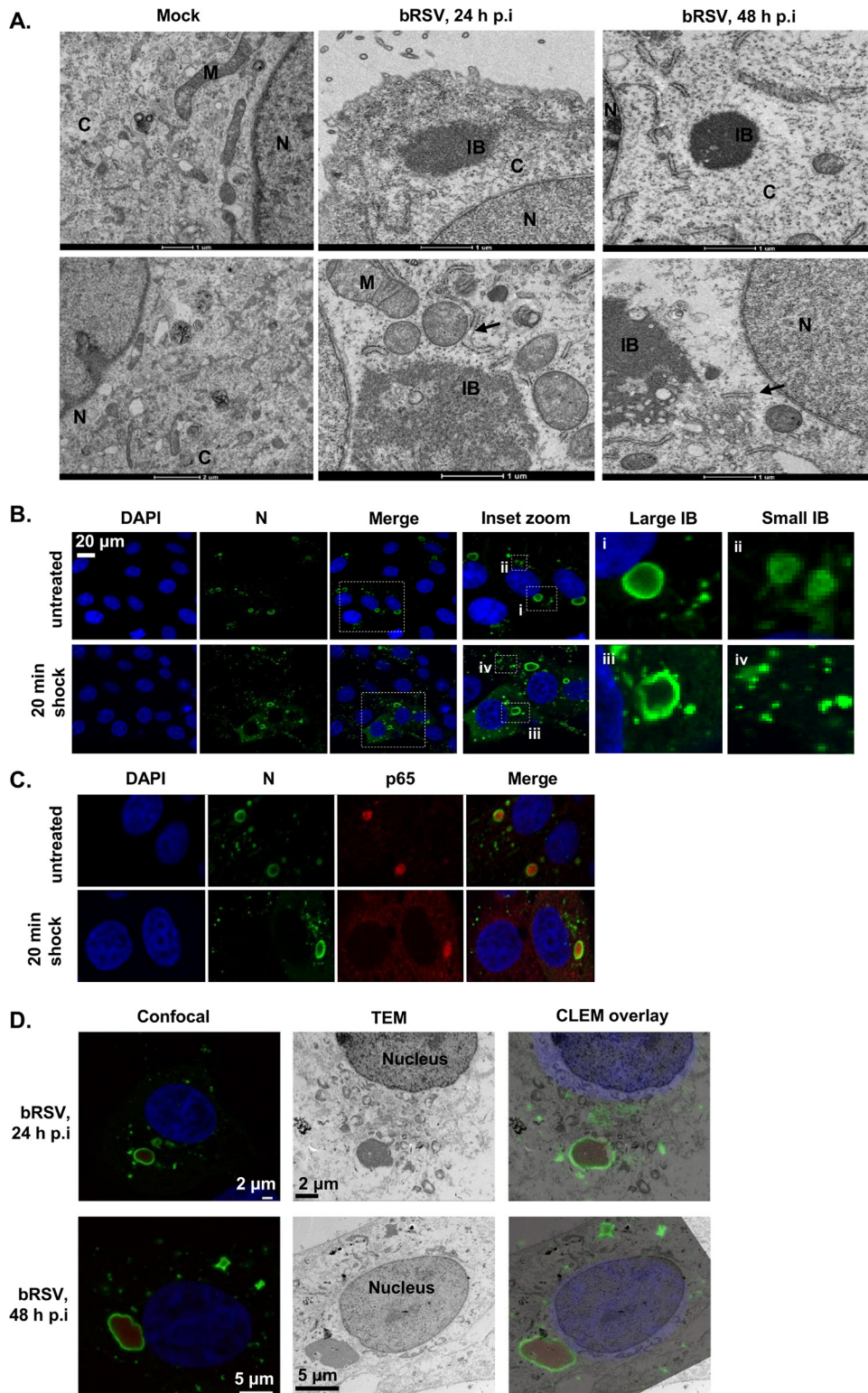
FIG 5 bRSV IBs are membraneless liquid organelles. (A) High-power transmission electron microscopy (TEM) of mock- or bRSV-infected Vero cells fixed in glutaraldehyde at 24 and 48 h p.i and prepared for TEM as detailed in the Materials and Methods. N, nucleus; M, mitochondria; C, cytoplasm; IB, inclusion body; ER is indicated with black arrow. Two representative images are shown per time point. Scale bars correspond to 1 μm. (B and C) Vero cells were infected with bRSV at an MOI of 1 and incubated at 37°C for 24 h. Hypotonic shock was applied for 20 min before the cells were fixed. Confocal analysis was performed following immunostaining for bRSV N (green) and nucleus stained with DAPI (and also p65 for C). Inset zooms demonstrate the observed effects of hypotonic shock on large (i and iii) and small (ii and iv) IBs—representative images shown. (D) Correlative light electron microscopy
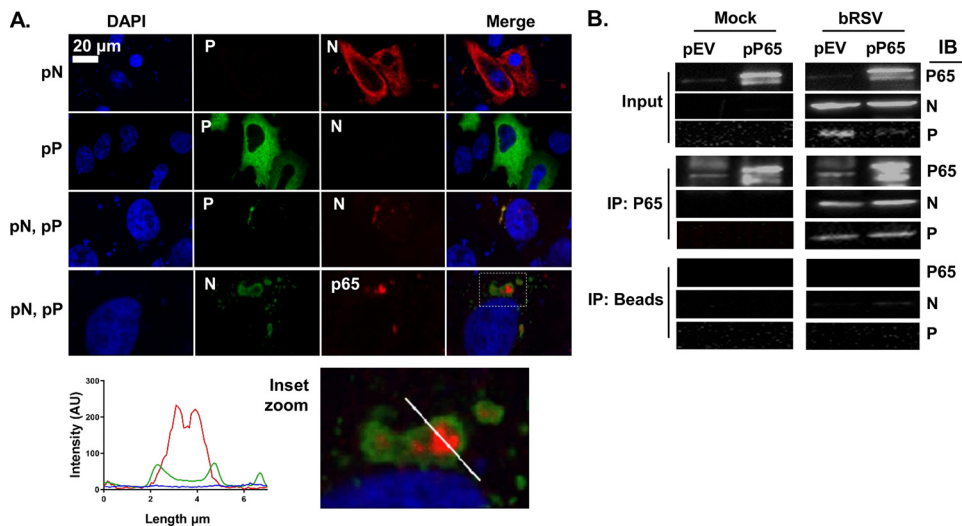
(Continued on next page)

FIG 6 Coexpression of bRSV N and P proteins induces the formation of IB-like structures which can sequester p65. (A) Vero cells were cotransfected with equimolar concentrations of plasmids expressing bRSV N (pN) and/or P (pP) proteins as indicated. Following 24 h of incubation, cells were fixed and stained with anti-RSV N (green/red) and anti-RSV P (green) or anti-NF-κB p65 (red) antibodies. Bottom image shows a higher magnification of the boxed area. Graph shows fluorescent intensity profiles along the indicated white line. (B) Coimmunoprecipitation of p65. 293T cells were transfected with plasmids expressing NF-κB p65 (pP65) or empty vector (pEV) and 6 h later infected with bRSV at an MOI of 1. At 24 h p.i., cell lysates were immunoprecipitated (IP) with anti-p65 antibody or beads alone as a control. Pulldowns were analyzed by SDS-PAGE and immunoblotting (IB) using anti-p65, anti-N, or anti-P antibodies.

p65 and N proteins localizing to the IB, with p65 present within the structure and N around the periphery. At 24 h p.i., the p65-positive IB structures were mostly spherical, becoming larger and more irregularly shaped by 48 h p.i., possibly as a result of transition into a more gel-like status, as discussed above. A similar pattern of immunostaining and IB morphology was also observed in bRSV-infected MDBK cells analyzed by CLEM (data not shown).

Coexpression of bRSV N and P proteins induces the formation of IB-like structures which can sequester p65. In the absence of infection, ectopic coexpression of many *Mononegavirales* N and P proteins has been shown to result in the formation of IB-like structures (24, 26, 28, 30)—a finding which has been linked to their potential to induce LLPS independently of viral infection. Although there has been broad discussion that this is related to the presence of intrinsically disordered regions within the N and P proteins, a definitive functional mechanism for this viral-induced LLPS remains uncharacterized. In addition, whether these infection-independent IB-like structures retain all the properties of viral IBs is not entirely clear. For hRSV, it was shown that IBAGs do not form within these visually orthologous bodies (26); however, the recruitment of MDA5 and MAVS to IB-like structures, following N and P overexpression, was maintained (24). To address similar questions for bRSV IBs and to examine the related sequestration of p65, Vero cells transiently transfected with plasmids expressing bRSV N (pN) and bRSV P (pP) were fixed and stained at 24 h posttransfection and examined by IF. As has been reported previously, the expression of N or P alone did not lead to the formation of IB-like structures; however, coexpression did, resulting in the formation of inclusions up to 6.9 μm² in area (Fig. 6A). Examination of the subcellular localization of p65 in this system also confirmed that the N- and P-induced inclusions were proficient in sequestering p65, independent of viral replication, with a

FIG 5 Legend (Continued)
(CLEM) of confocal microscopy immunostaining and TEM showing bRSV IBs. Vero cells infected with bRSV at an MOI of 1 were fixed at 24 or 48 h p.i., stained with antibodies against RSV N (green) and NF-κB p65 (red) and nuclei stained with DAPI. Following confocal imaging, cells were fixed in glutaraldehyde, sectioned, and visualized by TEM. Confocal (left) and TEM (middle) images of the same cells were overlaid (right) as CLEM images.

pattern of expression mirroring that seen in infected cells (Fig. 6A, inset zoom and fluorescent line of interest analysis).

To examine the mechanism of p65 recruitment to, and sequestration within, the bRSV IB, we next investigated whether there was evidence for direct protein-protein interactions between this protein and N or P. Endogenous p65 or p65 expressed from a plasmid (pP65) were immunoprecipitated from bRSV-infected or mock-infected 293T cells (at 24 h p.i.) using an anti-p65 antibody. When these immunoprecipitates were analyzed by Western blot, both bRSV N and P were found to coimmunoprecipitate (co-IP) with endogenous or overexpressed p65 in infected cell lysates, providing evidence of direct interactions being maintained postlysis (Fig. 6B). Experiments with beads alone did show a small amount of co-IP N protein; however, this amount was markedly lower than that in the p65 antibody experiment and may be background signal which we believe may be the consequence of the high levels of N protein in infected cells at 24 h p.i. In summary, our results indicate that p65 recruitment into bRSV IBs is maintained even in IB-like structures formed after N and P overexpression. Furthermore, the recruitment of p65 to IBs is likely due to specific interactions with the N and/or P proteins. Since RSV N and P are known to interact and yet the IB does not form without both proteins being expressed together, it is technically challenging to define the true binding partner, either N or P. As a result, more detailed characterization of this interaction is required to elucidate the mechanism of p65 sequestration.

The sequestration of the NF-κB subunit p65 to cytoplasmic IBs is a conserved mechanism of orthopneumovirus immunomodulation. Having established structural and functional similarity between bRSV and hRSV IBs, we finally examined the regulation and subcellular localization of the NF-κB subunit p65 in hRSV-infected cells. Beginning with the NF-κB luciferase reporter assay, we uncovered a pattern of signaling inhibition similar to bRSV. Infection with hRSV in the presence of the NF-κB reporter did not lead to robust activation compared with mock-infected cells, highlighting a lack of activation of this pathway in infected cells (Fig. 7A, black bars). Again, similar to bRSV, infected 293T cells (24 h with hRSV) which were stimulated for 6 h with hTNF-α induced significantly less NF-κB transactivation, compared with equivalently treated mock-infected cells (Fig. 7A, gray bars). This finding correlated well with an examination, by IF, of hRSV replication in Vero cells, with and without hTNF-α treatment, where again we did not observe significant levels of p65 nuclear translocation (Fig. 7B). Indeed, as observed in bRSV-infected cells, p65 was recruited into intracytoplasmic puncta. These puncta were subsequently shown to be synonymous with viral IBs (Fig. 7C) in a set of experiments which also confirmed that IB formation and the recruitment of p65 is host cell independent. bRSV- or hRSV-infected MDBK (bovine) or Hep2 (human) cells demonstrated the presence of p65-containing IBs in all scenarios, highlighting that the mechanisms underpinning RSV IB formation, and the sequestration of p65 to these bodies, are likely highly conserved (Fig. 7C). We concluded this examination of host-range specificity with a more physiologically relevant model of the human bronchial epithelium, BEAS-2B cells, which are derived from normal human tissues taken following autopsy of noncancerous individuals, identifying again the formation of IBs and sequestration of p65, regardless of RSV species. Finally, we confirmed that IB-like structures formed by ectopic hRSV N and P coexpression recruited p65 to their core (Fig. 7D). Taken together, these data indicate that the formation of IBs during viral replication, together with the sequestration of the transcription factor NF-κB subunit p65 to these bodies, is a common feature of orthopneumoviruses.

DISCUSSION

Recognition of viral pathogen-associated molecular patterns (PAMPs) by RIG-I or MDA5 can lead to activation of NF-κB transcription factors through the IKK complex or IRFs through TBK-1/IKKε (9, 11, 48). Activation of these innate responses is essential for inducing a robust adaptive response, first to clear viral infections and second to elicit the establishment of a memory response (4, 48). However, *in vivo*, the various immune-evasion strategies employed by RSV combine to generate only a short-lived response
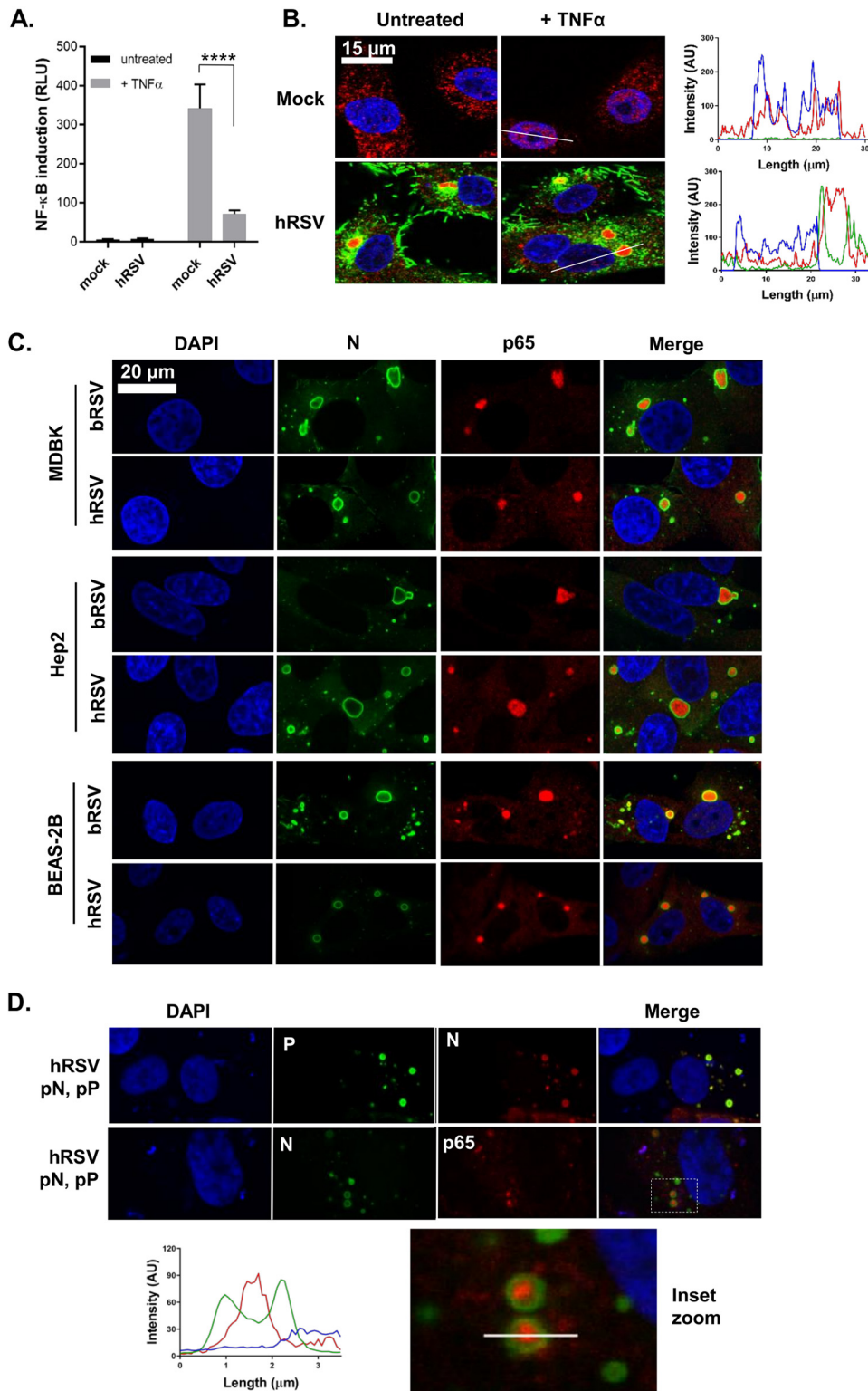
FIG 7 The sequestration of the NF-κB subunit p65 to cytoplasmic IBs is a conserved mechanism of orthopneumovirus immunomodulation. (A) 293T cells were mock-infected or infected with hRSV at an MOI of 1. At 6 h p.i., cells were transfected with 100-ng NF-κB FLuc reporter and 10-ng TK-renilla luciferase and incubated at 37°C. At 18 h p.t., cells were left untreated or stimulated for 16 h with 20 ng/ml hTNF-α. Cells were then lysed and analyzed for firefly and renilla luciferase activities. Graph depicts means ± SD of three replicates from the same experiment. Statistical significance determined by ANOVA as described in the Materials and Methods; ****, $P < 0.0001$. (B) Vero cells mock infected or infected with hRSV at an MOI of 1 for 24 h were left untreated or stimulated with 20 ng/ml hTNF-α for 30 min. Cells were then fixed and immunostained with anti-RSV F (green) or anti-NF-κB p65 (red) antibodies. Cell

(Continued on next page)

(4, 19, 20, 23, 48). For instance, there is strong evidence that the downregulation of key signaling molecules by the NS proteins suppresses IRF3 activation and type I IFN induction (17–20, 22, 23), although interestingly, we did see significant IRF3 nuclear translocation in our infected cells. As a key innate immune pathway, NF-κB signaling is often a target for viral antagonism; however, to date, RSV modulation of its activation has remained less well defined. Although RSV lacking the *SH* gene was shown to enhance NF-κB activation, the exact mechanisms employed are unclear (14, 15, 49, 50). To address this, we monitored NF-κB p65 activation in RSV-infected cells at multiple steps in the signaling pathway, namely, IκBα degradation, p65 phosphorylation (at Ser536), p65 nuclear translocation, and more broadly NF-κB transactivation. We present a novel mechanism of immune evasion wherein RSV infection results in the seques-tration of the NF-κB subunit p65 into viral inclusion bodies (Fig. 3B), a process which is independent of the known RSV immunomodulatory proteins NS1, NS2, and SH (Fig. 3F) and was confirmed in BEAS-2B bronchial epithelial cells for both hRSV and bRSV. The possibility that there is mechanistic redundancy between the RSV NS1, NS2, and SH accessory proteins cannot however be excluded at this time. We also demonstrate that as a result, activation of NF-κB p65 is suppressed in infected cells, even with exogenous TNF-α stimulation (Fig. 1). Although small IBs were observed as early as 6 h p.i. ($\leq$2.5 μm^2), they did not colocalize with detectable levels of p65 (Fig. 3E). This may reflect a technical limitation of our IF or alternatively that IBs need to grow in size before they can begin to sequester p65. It remains to be determined if p65 is actively recruited to IBs by viral proteins or if its sequestration is a result of the IB's position in the cell and that it captures p65 by an indirect mechanism, perhaps involving trafficking. In addi-tion, it is currently not clear what proportion of the IB-sequestered p65 is IκBα associated, the elucidation of which might explain the partial protection of IκBα from degradation seen following TNF-α treatment (Fig. 1D, mock versus bRSV +TNF-α). Interestingly, the lack of p65 activation prior to IB formation and p65 aggregation highlights that RSV may employ additional mechanisms for NF-κB inhibition which remain uncharacterized. Other groups have reported more robust activation of NF-κB in response to RSV infection (7, 51, 52) which could indicate that the cell line and viral strain play a role in RSV-mediated NF-κB activation. This being said, the sequestration of p65 appears to be an orthopneumovirus-conserved strategy active in physiologically relevant cells, such as BEAS-2Bs. From a wider perspective, this mechanism of immu-nomodulation might be a common strategy utilized by RSV and other viruses that induce IB formation. MAVS and MDA5 were similarly both found to be recruited into RSV IBs as a mechanism of suppressing IFN signaling (24). Similarly, p38 MAPK and OGT sequestration into RSV IBs suppressed MAPK-activated protein kinase 2 signaling and stress granule formation, respectively, enhancing virus replication (25). Whether viruses such as Ebola, Nipah, or rabies adopt similar mechanisms of immunomodulation remains to be determined.

From a mechanistic perspective, our results also showed that the N and P proteins are essential for the formation of bRSV IBs. As has been reported for rabies (28) and measles (30) viruses, ectopic expression of these proteins resulted in the formation of IB-like structures (Fig. 6A and 7D). They were mostly spherical and, at 24 h posttrans-fection, measured up to 6.9 μm^2 which is considerably less than that of the conven-tional IBs observed in infected cells. We hypothesize that both pseudo-IBs and viral IBs form by biomolecular condensation but that their maturation into larger structures is

FIG 7 Legend (Continued)
nuclei were stained with DAPI (blue) and images obtained using a Leica TCS SP5 confocal microscope. Graphs show line fluorescent intensity profiles along the indicated white lines. (C) MDBK, Hep2, and BEAS-2B cells were infected with b/hRSV for 24 h, fixed, and immunostained for RSV N (green) or NF-κB p65 (red). (D) Vero cells were cotransfected with equimolar concentrations of plasmids expressing hRSV N (pN) and/or P (pP) proteins as indicated. Following 24 h of incubation, cells were fixed and stained with anti-RSV N (green/red) and anti-RSV P (green) or anti-NF-κB p65 (red) antibodies. Cell nuclei were stained with DAPI (blue) and confocal analysis performed. The bottom image shows a higher magnification of the boxed area, and the graph shows the fluorescent intensity profiles along the indicated white line.

dependent on other factors present only in infected cells. That these pseudo-IBs could also recruit p65 suggested a direct interaction between p65 and RSV N or P, which we confirmed by co-IP (Fig. 6B). Interestingly, our IF data were somewhat contradictory, with the staining patterns and line intensity profiles showing p65 concentrated in the middle of IBs with N and P at the periphery, separating the IB contents from the cytoplasm. It is possible that the exchange of biomolecules across the boundary, e.g., during the sequestration of p65, may require transient N or P interactions. Intriguingly, Lifland et al. also suggested that MAVS and MDA5 are recruited into IBs by interacting with N and P in a macromolecular complex (24). We propose that this recruitment may involve low-affinity interactions with N and/or P and that maintenance within the IB is enhanced by the same physicochemical properties of the IBs which enable them to induce LLPS, namely, macromolecule-macromolecule interactions. The RSV P protein has been shown to bind and recruit M2-1 to IBs, potentially through intrinsically disordered regions within P that allow it to form multiple interactions (53). Although further work is required to identify the exact mechanism of p65, MAVS, and MDA5 recruitment into IBs, we postulate that the physicochemical properties of these proteins may also be an important factor. Of note, in order to definitively identify the bRSV IBs as liquid organelles, fluorescence recovery after photobleaching (FRAP) experiments could be performed to assess the acquisition of tagged N or P over time. In addition, the fusion and fission of these organelles could be monitored in real time. Both of these experimental approaches are areas of continued investigation in our laboratory; however, the dissolution of the smaller IBs in response to hypotonic shock still provides strong evidence for the LLPS nature of these structures (Fig. 5B). The stability of larger IBs to extended periods of hypotonic shock was surprising—a finding we attribute to the larger IBs gaining hydrogel- or even aggregate-like status. This might also explain the loss of their spherical nature, as the biophysical constraints on this organelle might be relaxed by this transition.

Electron micrograph analysis of our RSV IBs showed greater electron density in the IBs than in the cytoplasm, a characteristic of biomolecular condensates (Fig. 5A). These data also highlighted the structural complexity of the phase-separated structure. Although we observed some association with the ER and RER, RSV IBs were not membrane bound, unlike rabies virus negri bodies which acquire a membrane boundary later in infection, presumably derived from the ER (28, 39). Interestingly, our CLEM analysis confirmed previous IF data from the field that the IB boundary is surrounded by N protein (Fig. 5D). A debate remains in the field as to whether this is an artifact of disrupted antibody epitope accessibility to N since GFP-tagged N proteins were shown to have a diffuse pattern throughout the IB (24); however, we would only note that we used an antibody developed in-house for this staining. Nevertheless, the presence of viral RNA-associated proteins N, P, and M2-1 in IBs (Fig. 3B and 4C) strongly suggested the presence of RNA replication and transcription within these structures. Building on previous work for hRSV and rabies virus (26, 39), we used 5EU incorporation to confirm RNA synthesis in the IBs (Fig. 4A and B). Using fluorescence in situ hybridization (FISH) experiments, Rincheval et al. showed that genomic RNA colocalized with the hRSV N and P proteins at the periphery, while viral mRNA was found to concentrate in IBAGs, transient sites of mRNA storage (26). Our data showed the formation of similar structures, confirming IBAGs are found in multiple orthopneumoviruses; however, there was no conclusive colocalization with p65. However, this sequestered cellular protein did localize to distinct intra-IB bodies (Fig. 4B and C), raising the intriguing possibility that multiple microdomains exist within what is, by TEM, an apparently uniform granular biomolecular condensate.

In summary, our data show that RSV IBs are highly ordered structures performing multiple roles in the virus life cycle, including the compartmentalization of virus replication and transcription and the sequestration of cellular proteins involved in the antiviral response. This mechanistic characterization is potentially applicable to other negative-sense RNA viruses that have been shown to form IBs during replication.

MATERIALS AND METHODS

Cells and viruses. All cells were cultured at 37°C in a 5% CO_2 atmosphere. Madin-Darby bovine kidney (MDBK), Vero (monkey kidney epithelial), 293T (human embryonic kidney), and Hep-2 (human epithelial type 2) cells were obtained from the Pirbright Institute Central Services Unit and maintained in Dulbecco's modified Eagle's medium (DMEM) supplemented with 10% heat-inactivated fetal calf serum (FCS; TCS Biologicals), sodium pyruvate (Gibco), and penicillin and streptomycin (Sigma). Beas-2B (human bronchial epithelial) cells (ATCC) were cultured in LHC basal medium (ThermoFisher) supplemented with 10% FCS, penicillin, and streptomycin.

Wild-type recombinant bRSV (rbRSV) and deletion mutant rbRSVs ΔSH, ΔNS1, ΔNS2, and ΔNS1/2 were produced by reverse genetics from rbRSV strain A51908 variant Atue51908 (GenBank accession no. AF092942) (18, 40, 54). They were propagated in Vero cells and hRSV subtype A (A2 strain) grown in Hep-2 cells. All viruses were further purified from total cell lysates using polyethylene glycol (molecular weight, 8,000) precipitation and discontinuous sucrose gradient centrifugation.

Plasmids and transfections. All viral gene sequences were derived from bRSV A51908 (GenBank accession no. NC_038272) and hRSV A2 (GenBank accession no. KT992094). Expression plasmids (pcDNA3.1) encoding codon-optimized N genes at KpnI-BamHI sites referred to as pN were purchased from Bio Basic Inc. Full-length P genes were amplified by reverse transcriptase PCR using gene-specific primers and Superscript II reverse transcriptase (Invitrogen). They were then cloned into pcDNA3.1 at KpnI-BamHI sites and designated pP. The p65 open reading frame (ORF) was amplified from pcDNA3.1-HA-p65 (kindly provided by Carlos Maluquer de Motes, University of Surrey), inserted at the HindIII-BamHI sites of pcDNA3.1, and designated pP65. All sequences were confirmed by conventional sanger sequencing. Plasmids were transfected into cells using TransIT-X2 (Geneflow).

Antibodies and drugs. Mouse monoclonal antibodies raised against bRSV F (mAb19), N (mAb89), P (mAb12), M (mAb105), and M2-1 (mAb91) were previously described (55, 56). The rabbit polyclonal anti-bRSV SH antibody was purchased from Ingenasa. Rabbit anti-NF-κB p65 (8242) antibody, rabbit anti-IRF3 (11904), rabbit anti-phospho-NF-κB p65 (Ser536; 3033), mouse anti-IκBα (4814), and rabbit anti-GAPDH (5174) were obtained from Cell Signaling Technology (CST). Mouse anti-G3BP-1 was obtained from BD Biosciences. Secondary horseradish peroxidase-linked antibodies were obtained from CST and Alexa Fluor secondary antibodies from Life Technologies. Recombinant hTNF-α (CST), poly(I:C) (InvivoGen), sodium arsenite (Sigma), and actinomycin D (Sigma) were purchased from the indicated suppliers.

Confocal immunofluorescence microscopy. Cells were fixed with 4% paraformaldehyde (PFA; Sigma) in PBS for 15 min, permeabilized with 0.2% Triton X-100 in PBS for 5 min, and blocked with 0.5% bovine serum albumin (BSA) (Sigma) in PBS. Cells were then incubated with the indicated primary antibodies overnight at 4°C. They were then washed and incubated with Alexa Fluor secondary antibodies (Life Technologies) for 1 h at room temperature. Cells were then washed and mounted with Vectashield (Vector labs) containing 4',6-diamidino-2-phenylindole (DAPI) for nuclei staining. Fluorescence was imaged on a Leica TCS SP5 confocal microscope using 405-nm, 488-nm, and 568-nm laser lines for the appropriate dyes and a 63× oil immersion objective.

Quantitation of bRSV-induced p65 puncta and IBs. Mock- or bRSV-infected (at an MOI of 1) MDBK cells were fixed in 4% PFA (Sigma) at 6, 16, and 24 h p.i. and labeled according to the described immunofluorescence method. Multiple Z-sections, 0.5 μm apart, were taken for each cell, by confocal microscopy and max intensity Z-stacks of 8 planes made using the Leica LAS AF Lite software. Quantifications of N- and p65-positive structures were performed using the area region of interest analysis tool. GraphPad Prism 7 was used to perform parametric one-way analysis of variance (ANOVA) and Tukey's multiple comparison tests. ImageJ was also used to make 3D projections of 9 images 0.9 μm apart.

Luciferase reporter assay. A total of 2×10^5 293T cells seeded onto 24-well plates a day prior were mock infected or infected with bRSV or hRSV at an MOI of 1. A total of 6 h later, cells were cotransfected with a 100-ng NF-κB FLuc reporter which expresses the firefly luciferase gene under the control of five NF-κB repeated transcription factor binding sites and 10-ng TK-ren control plasmid (both kindly provided by Gareth Brady; The University of Dublin) using Transit-X2 (Geneflow). A total of 24 hours later, cells were stimulated with 20 ng/ml hTNF-α for 16 hours or were left untreated. Cells were then lysed with reporter lysis buffer (Promega), and lysates were used to determine firefly and renilla luciferase activities on a Glomax luminometer using the luciferase assay system (Promega) and coeleterazine (Promega), respectively. Firefly data were normalized to renilla which was used as an internal control of transfection. GraphPad Prism 7 was used to perform parametric one-way analysis of variance (ANOVA) and Tukey's multiple comparison tests.

Western blot analysis. Following virus infection and stimulation, growth medium was removed from cells and cell extracts prepared by lysis in SDS sample buffer (Bio-Rad) supplemented with β-mercaptoethanol (Sigma), complete mini-EDTA-free protease inhibitors (Roche), and 1 mM sodium orthovanadate (New England BioLabs). Lysates were then boiled for 5 min and 30 μl resolved by SDS-PAGE on a 12% polyacrylamide gel and proteins transferred to polyvinylidene difluoride (PVDF) membranes (ThermoScientific). After being blocked for 1 h with 5% dry semiskimmed milk in 0.1% PBS Tween 20 (PBS-T), membranes were washed with PBS-T and incubated with primary antibodies overnight at 4°C. After being washed, the membranes were incubated with the corresponding horseradish peroxidase-conjugated secondary antibodies (CST). Protein bands were detected using Clarity Western ECL substrate (Bio-Rad) and imaged with the Bio-Rad ChemiDoc MP imaging system.

5-Ethynyl uridine labeling. Infected cells growing on coverslips were incubated with or without medium supplemented with 20 μg/ml actinomycin D (Act D) to inhibit cellular transcription for 1 h. Cells

were then incubated with medium containing 1 mM 5EU and 20 μg/ml Act D for another hour. Medium was then washed off and cells fixed in 4% PFA for 15 min. Cells were then washed with PBS and permeabilized with 0.2% Triton X-100 for 5 min. They were both supplemented with 0.125 U/ml RNase inhibitor (Promega). Incorporated 5EU was labeled using the Click-IT RNA imaging kit (Invitrogen) following the manufacturer's protocol. Following that step, immunofluorescence staining was done as described above.

Transmission electron microscopy. Cells seeded onto Thermanox coverslips (Thermo Scientific) were fixed at 24 h and 48 h p.i in phosphate-buffered 2% glutaraldehyde (Agar Scientific) for 1 hour followed by 1 hour in aqueous 1% osmium tetroxide (Agar Scientific). We performed the following dehydration steps in an ethanol series: 70% for 30 min, 90% for 15 min, and 100% three times for 10 min. Then, a transitional step of 10 min in propylene oxide (Agar Scientific) was undertaken before infiltration with a 50:50 mix of propylene oxide and epoxy resin (Agar Scientific) for 1 hour. After a final infiltration of 100% epoxy resin for 1 hour, the samples were embedded and polymerized overnight at 60°C. Next, 80-μm-thin sections were cut, collected onto copper grids (Agar Scientific), and grid stained using Leica EM AC20 before being imaged at 100 kV in a FEI Tecnai 12 TEM with a TVIPS F214 digital camera.

Correlative light electron microscopy. Cells seeded onto gridded glass coverslips (MatTek) were fixed at 24 h and 48 h p.i in 4% PFA (Sigma) and labeled according to the described immunofluorescence method. Selected grid squares were imaged on a Leica TCS SP8 confocal microscope using 405-nm, 488-nm, and 568-nm laser lines for the appropriate dyes. The cells were then fixed in phosphate-buffered 2% glutaraldehyde (Agar Scientific) for 1 hour followed by 1 hour in aqueous 1% osmium tetroxide (Agar Scientific). Following 15 min in 3% uranyl acetate (Agar Scientific), the cells were dehydrated in an ethanol series, as follows: 70% for 30 min, 90% for 15 min, and 100% three times for 10 min. After infiltration of 100% epoxy resin for 2 hours, the samples were embedded and polymerized overnight at 60°C. The glass coverslips were removed with liquid nitrogen and the appropriate grid squares located. Next, 80-μm-thin sections were cut, collected onto copper grids (Agar Scientific), and grid stained using a Leica EM AC20 instrument. The specific cells imaged in the confocal were identified and imaged at 100 kV in a FEI Tecnai 12 TEM with a TVIPS F214 digital camera.

Coimmunoprecipitation. A total of 1×10^5 293T cells cultured overnight in 12-well plates were transfected with pcDNA3.1-empty vector (pEV) or pcDNA3.1-p65 (pP65) using the TransIT-X2 reagent (Geneflow). After 24 h, cells were infected with bRSV at an MOI of 1 or mock infected and incubated for another 24 h. Cells were then lysed on ice with radioimmunoprecipitation assay (RIPA) lysis buffer (EMB Millipore) and cell debris removed by centrifugation. Cell lysates precleared with protein A-coated magnetic beads (CST) were incubated with rabbit anti-p65 antibodies overnight at 4°C. Lysates were then incubated with protein A-coated magnetic beads for 20 min at room temperature with rotation. Following five washes with PBS-T, immunoprecipitates were eluted with Laemmli sample buffer and subjected to SDS-PAGE and Western blot analysis as already described.

Ethics statement. This research did not use any primary human or animal tissue. BEAS-2B cells were procured from ATCC.

SUPPLEMENTAL MATERIAL

Supplemental material is available online only.
SUPPLEMENTAL FILE 1, AVI file, 0.3 MB.
SUPPLEMENTAL FILE 2, AVI file, 1.4 MB.
SUPPLEMENTAL FILE 3, PDF file, 0.01 MB.

REFERENCES

1. Hogan AB, Glass K, Moore HC, Anderssen RS. 2016. Exploring the dynamics of respiratory syncytial virus (RSV) transmission in children. Theor Popul Biol 110:78–85. https://doi.org/10.1016/j.tpb.2016.04.003.

2. Falsey AR, Hennessey PA, Formica MA, Cox C, Walsh EE. 2005. Respiratory syncytial virus infection in elderly and high-risk adults. N Engl J Med 352:1749–1759. https://doi.org/10.1056/NEJMoa043951.

3. Habibi MS, Jozwik A, Makris S, Dunning J, Paras A, Mechanisms of Severe Acute Influenza Consortium Investigators, DeVincenzo JP, de Haan CAM, Wrammert J, Openshaw PJM, Chiu C. 2015. Impaired antibody-mediated protection and defective IgA B-cell memory in experimental infection of adults with respiratory syncytial virus. Am J Respir Crit Care Med 191:1040–1049. https://doi.org/10.1164/rccm.201412-2256OC.

4. Guzman E, Taylor G. 2015. Immunology of bovine respiratory syncytial virus in calves. Mol Immunol 66:48–56. https://doi.org/10.1016/j.molimm.2014.12.004.

5. Amarasinghe GK, Bào Y, Basler CF, Bavari S, Beer M, Bejerman N, Blasdell KR, Bochnowski A, Briese T, Bukreyev A, Calisher CH, Chandran K, Collins PL, Dietzgen RG, Dolnik O, Dürrwald R, Dye JM, Easton AJ, Ebihara H, Fang Q, Formenty P, Fouchier RAM, Ghedin E, Harding RM, Hewson R, Higgins CM, Hong J, Horie M, James AP, Jiãng D, Kobinger GP, Kondo H, Kurath G, Lamb RA, Lee B, Leroy EM, Li M, Maisner A, Mühlberger E, Netesov SV, Nowotny N, Patterson JL, Payne SL, Paweska JT, Pearson MN, Randall RE, Revill PA, Rima BK, Rota P, Rubbenstroth D, Schwellme M, Smither SJ, Song Q, Stone DM, Takada A, Terregino C, Tesh RB, Tomonaga K, Tordo N, Towner JS, Vasilakis N, Volchknov VE, Wahl-Jensen V, Walker PJ, Wang B, Wang D, Wang F, Wang L-F, Werren JH, Whitfield AE, Yan Z, Ye G, Kuhn JH. 2017. Taxonomy of the order Mononegavirales: update 2017. Arch Virol 162:2493–2504. https://doi.org/10.1007/s00705-017-3311-7.

6. Liu P, Jamaluddin M, Li K, Garofalo RP, Casola A, Brasier AR. 2007. Retinoic acid-inducible gene I mediates early antiviral response and Toll-like receptor 3 expression in respiratory syncytial virus-infected airway epithelial cells. J Virol 81:1401–1411. https://doi.org/10.1128/JVI.01740-06.

7. Yoboua F, Martel A, Duval A, Mukawera E, Grandvaux N. 2010. Respiratory syncytial virus-mediated NF-kappa B p65 phosphorylation at serine 536 is dependent on RIG-I, TRAF6, and IKK beta. J Virol 84:7267–7277. https://doi.org/10.1128/JVI.00142-10.

8. Baum A, García-Sastre A. 2010. Induction of type I interferon by RNA viruses: cellular receptors and their substrates. Amino Acids 38:1283–1299. https://doi.org/10.1007/s00726-009-0374-0.

9. Mitchell S, Vargas J, Hoffmann A. 2016. Signaling via the NFkappaB system. Wiley Interdiscip Rev Syst Biol Med 8:227–241. https://doi.org/10.1002/wsbm.1331.

10. Kanarek N, Ben-Neriah Y. 2012. Regulation of NF-kappaB by ubiquitination and degradation of the IkappaBs. Immunol Rev 246:77–94. https://doi.org/10.1111/j.1600-065X.2012.01098.x.

11. Hemmi H, Takeuchi O, Sato S, Yamamoto M, Kaisho T, Sanjo H, Kawai T, Hoshino K, Takeda K, Akira S. 2004. The roles of two IkappaB kinase-related kinases in lipopolysaccharide and double stranded RNA signaling and viral infection. J Exp Med 199:1641–1650. https://doi.org/10.1084/jem.20040520.

12. Deng L, Zeng Q, Wang M, Cheng A, Jia R, Chen S, Zhu D, Liu M, Yang Q, Wu Y, Zhao X, Zhang S, Liu Y, Yu Y, Zhang L, Chen X. 2018. Suppression of NF-kappaB activity: a viral immune evasion mechanism. Viruses 10:409. https://doi.org/10.3390/v10080409.

13. Chiang H-S, Liu HM. 2018. The molecular basis of viral inhibition of IRF- and STAT-Dependent immune responses. Front Immunol 9:3086. https://doi.org/10.3389/fimmu.2018.03086.

14. Pollock N, Taylor G, Jobe F, Guzman E. 2017. Modulation of the transcription factor NF-kappaB in antigen-presenting cells by bovine respiratory syncytial virus small hydrophobic protein. J Gen Virol 98:1587–1599. https://doi.org/10.1099/jgv.0.000855.

15. Taylor G, Wyld S, Valarcher J-F, Guzman E, Thom M, Widdison S, Buchholz UJ. 2014. Recombinant bovine respiratory syncytial virus with deletion of the SH gene induces increased apoptosis and pro-inflammatory cytokines in vitro, and is attenuated and induces protective immunity in calves. J Gen Virol 95:1244–1254. https://doi.org/10.1099/vir.0.064931-0.

16. Spann KM, Tran KC, Chi B, Rabin RL, Collins PL. 2004. Suppression of the induction of alpha, beta, and lambda interferons by the NS1 and NS2 proteins of human respiratory syncytial virus in human epithelial cells and macrophages. J Virol 78:4363–4369. https://doi.org/10.1128/jvi.78.8.4363-4369.2004.

17. Spann KM, Tran KC, Collins PL. 2005. Effects of nonstructural proteins NS1 and NS2 of human respiratory syncytial virus on interferon regulatory factor 3, NF-kappaB, and proinflammatory cytokines. J Virol 79:5353–5362. https://doi.org/10.1128/JVI.79.9.5353-5362.2005.

18. Schlender J, Bossert B, Buchholz U, Conzelmann KK. 2000. Bovine respiratory syncytial virus nonstructural proteins NS1 and NS2 cooperatively antagonize alpha/beta interferon-induced antiviral response. J Virol 74:8234–8242. https://doi.org/10.1128/jvi.74.18.8234-8242.2000.

19. Lo MS, Brazas RM, Holtzman MJ. 2005. Respiratory syncytial virus nonstructural proteins NS1 and NS2 mediate inhibition of Stat2 expression and alpha/beta interferon responsiveness. J Virol 79:9315–9319. https://doi.org/10.1128/JVI.79.14.9315-9319.2005.

20. Ling Z, Tran KC, Teng MN. 2009. Human respiratory syncytial virus nonstructural protein NS2 antagonizes the activation of beta interferon transcription by interacting with RIG-I. J Virol 83:3734–3742. https://doi.org/10.1128/JVI.02434-08.

21. Boyapalle S, Wong T, Garay J, Teng M, San Juan-Vergara H, Mohapatra S, Mohapatra S. 2012. Respiratory syncytial virus NS1 protein colocalizes with mitochondrial antiviral signaling protein MAVS following infection. PLoS One 7:e29386. https://doi.org/10.1371/journal.pone.0029386.

22. Goswami R, Majumdar T, Dhar J, Chattopadhyay S, Bandyopadhyay SK, Verbovetskaya V, Sen GC, Barik S. 2013. Viral degradasome hijacks mitochondria to suppress innate immunity. Cell Res 23:1025–1042. https://doi.org/10.1038/cr.2013.98.

23. Kotelkin A, Belyakov IM, Yang L, Berzofsky JA, Collins PL, Bukreyev A. 2006. The NS2 protein of human respiratory syncytial virus suppresses the cytotoxic T-cell response as a consequence of suppressing the type I interferon response. J Virol 80:5958–5967. https://doi.org/10.1128/JVI.00181-06.

24. Lifland AW, Jung J, Alonas E, Zurla C, Crowe JE, Jr, Santangelo PJ. 2012. Human respiratory syncytial virus nucleoprotein and inclusion bodies antagonize the innate immune response mediated by MDA5 and MAVS. J Virol 86:8245–8258. https://doi.org/10.1128/JVI.00215-12.

25. Fricke J, Koo LY, Brown CR, Collins PL. 2013. p38 and OGT sequestration into viral inclusion bodies in cells infected with human respiratory syncytial virus suppresses MK2 activities and stress granule assembly. J Virol 87:1333–1347. https://doi.org/10.1128/JVI.02263-12.

26. Rincheval V, Lelek M, Gault E, Bouillier C, Sitterlin D, Blouquit-Laye S, Galloux M, Zimmer C, Eleouet JF, Rameix-Welti MA. 2017. Functional organization of cytoplasmic inclusion bodies in cells infected by respiratory syncytial virus. Nat Commun 8:563. https://doi.org/10.1038/s41467-017-00655-9.

27. Nikolic J, Civas A, Lama Z, Lagaudriere-Gesbert C, Blondel D. 2016. Rabies virus infection induces the formation of stress granules closely connected to the viral factories. PLoS Pathog 12:e1005942. https://doi.org/10.1371/journal.ppat.1005942.

28. Nikolic J, Le Bars R, Lama Z, Scrima N, Lagaudriere-Gesbert C, Gaudin Y, Blondel D. 2017. Negri bodies are viral factories with properties of liquid organelles. Nat Commun 8:58. https://doi.org/10.1038/s41467-017-00102-9.

29. Cifuentes-Muñoz N, Branttie J, Slaughter KB, Dutch RE. 2017. Human metapneumovirus induces formation of inclusion bodies for efficient genome replication and transcription. J Virol 91:e01282-17. https://doi.org/10.1128/JVI.01282-17.

30. Zhou Y, Su JM, Samuel CE, Ma D. 2019. Measles virus forms inclusion bodies with properties of liquid organelles. J Virol 93:e00948-19. https://doi.org/10.1128/JVI.00948-19.

31. Garcia J, Garcia-Barreno B, Vivo A, Melero JA. 1993. Cytoplasmic inclusions of respiratory syncytial virus-infected cells: formation of inclusion bodies in transfected cells that coexpress the nucleoprotein, the phosphoprotein, and the 22K protein. Virology 195:243–247. https://doi.org/10.1006/viro.1993.1366.

32. Ringel M, Heiner A, Behner L, Halwe S, Sauerhering L, Becker N, Dietzel E, Sawatsky B, Kolesnikova L, Maisner A. 2019. Nipah virus induces two inclusion body populations: identification of novel inclusions at the plasma membrane. PLoS Pathog 15:e1007733. https://doi.org/10.1371/journal.ppat.1007733.

33. White JP, Lloyd RE. 2012. Regulation of stress granules in virus systems. Trends Microbiol 20:175–183. https://doi.org/10.1016/j.tim.2012.02.001.

34. Lindquist ME, Lifland AW, Utley TJ, Santangelo PJ, Crowe JE, Jr. 2010.

Respiratory syncytial virus induces host RNA stress granules to facilitate viral replication. J Virol 84:12274–12284. https://doi.org/10.1128/JVI.00260-10.

35. Hanley LL, McGivern DR, Teng MN, Djang R, Collins PL, Fearns R. 2010. Roles of the respiratory syncytial virus trailer region: effects of mutations on genome production and stress granule formation. Virology 406: 241–252. https://doi.org/10.1016/j.virol.2010.07.006.

36. Lindquist ME, Mainou BA, Dermody TS, Crowe JE, Jr. 2011. Activation of protein kinase R is required for induction of stress granules by respiratory syncytial virus but dispensable for viral replication. Virology 413: 103–110. https://doi.org/10.1016/j.virol.2011.02.009.

37. Ghildyal R, Mills J, Murray M, Vardaxis N, Meanger J. 2002. Respiratory syncytial virus matrix protein associates with nucleocapsids in infected cells. J Gen Virol 83:753–757. https://doi.org/10.1099/0022-1317-83-4-753.

38. Shahriari S, Wei KJ, Ghildyal R. 2018. Respiratory syncytial virus matrix (M) protein interacts with actin in vitro and in cell culture. Viruses 10:535. https://doi.org/10.3390/v10100535.

39. Lahaye X, Vidy A, Pomier C, Obiang L, Harper F, Gaudin Y, Blondel D. 2009. Functional characterization of Negri bodies (NBs) in rabies virus-infected cells: evidence that NBs are sites of viral transcription and replication. J Virol 83:7948–7958. https://doi.org/10.1128/JVI.00554-09.

40. Buchholz UJ, Finke S, Conzelmann KK. 1999. Generation of bovine respiratory syncytial virus (BRSV) from cDNA: BRSV NS2 is not essential for virus replication in tissue culture, and the human RSV leader region acts as a functional BRSV genome promoter. J Virol 73:251–259. https://doi.org/10.1128/JVI.73.1.251-259.1999.

41. Carromeu C, Simabuco FM, Tamura RE, Farinha Arcieri LE, Ventura AM. 2007. Intracellular localization of human respiratory syncytial virus L protein. Arch Virol 152:2259–2263. https://doi.org/10.1007/s00705-007-1048-4.

42. Alberti S, Gladfelter A, Mittag T. 2019. Considerations and challenges in studying liquid-liquid phase separation and biomolecular condensates. Cell 176:419–434. https://doi.org/10.1016/j.cell.2018.12.035.

43. Murthy AC, Fawzi NL. 2020. The (un)structural biology of biomolecular liquid-liquid phase separation using NMR spectroscopy. J Biol Chem 295:2375–2384. https://doi.org/10.1074/jbc.REV119.009847.

44. Mudogo CN, Falke S, Brognaro H, Duszenko M, Betzel C. 2020. Protein phase separation and determinants of in cell crystallization. Traffic 21: 220–230. https://doi.org/10.1111/tra.12711.

45. Perez-Pepe M, Fernandez-Alvarez AJ, Boccaccio GL. 2018. Life and work of stress granules and processing bodies: new insights into their formation and function. Biochemistry 57:2488–2498. https://doi.org/10.1021/acs.biochem.8b00025.

46. Nikolic J, Lagaudriere-Gesbert C, Scrima N, Blondel D, Gaudin Y. 2018. [Rabies virus factories are formed by liquid-liquid phase separation]. Med Sci (Paris) 34:203–205. https://doi.org/10.1051/medsci/20183403004.

47. Shin Y, Berry J, Pannucci N, Haataja MP, Toettcher JE, Brangwynne CP. 2017. Spatiotemporal control of intracellular phase transitions using light-activated optoDroplets. Cell 168:159–171.e14. https://doi.org/10.1016/j.cell.2016.11.054.

48. Sun Y, Lopez CB. 2017. The innate immune response to RSV: advances in our understanding of critical viral and host factors. Vaccine 35:481–488. https://doi.org/10.1016/j.vaccine.2016.09.030.

49. Russell RF, McDonald JU, Ivanova M, Zhong Z, Bukreyev A, Tregoning JS. 2015. Partial attenuation of respiratory syncytial virus with a deletion of a small hydrophobic gene is associated with elevated interleukin-1beta responses. J Virol 89:8974–8981. https://doi.org/10.1128/JVI.01070-15.

50. Fuentes S, Tran KC, Luthra P, Teng MN, He B. 2007. Function of the respiratory syncytial virus small hydrophobic protein. J Virol 81: 8361–8366. https://doi.org/10.1128/JVI.02717-06.

51. Bitko V, Garmon NE, Cao T, Estrada B, Oakes JE, Lausch RN, Barik S. 2004. Activation of cytokines and NF-kappa B in corneal epithelial cells infected by respiratory syncytial virus: potential relevance in ocular inflammation and respiratory infection. BMC Microbiol 4:28. https://doi.org/10.1186/1471-2180-4-28.

52. Carpenter LR, Moy JN, Roebuck KA. 2002. Respiratory syncytial virus and TNF alpha induction of chemokine gene expression involves differential activation of Rel A and NF-kappa B1. BMC Infect Dis 2:5. https://doi.org/10.1186/1471-2334-2-5.

53. Richard CA, Rincheval V, Lassoued S, Fix J, Cardone C, Esneau C, Nekhai S, Galloux M, Rameix-Welti MA, Sizun C, Eleouet JF. 2018. RSV hijacks cellular protein phosphatase 1 to regulate M2-1 phosphorylation and viral transcription. PLoS Pathog 14:e1006920. https://doi.org/10.1371/journal.ppat.1006920.

54. Karger A, Schmidt U, Buchholz UJ. 2001. Recombinant bovine respiratory syncytial virus with deletions of the G or SH genes: G and F proteins bind heparin. J Gen Virol 82:631–640. https://doi.org/10.1099/0022-1317-82-3-631.

55. Taylor G, Stott EJ, Bew M, Fernie BF, Cote PJ, Collins AP, Hughes M, Jebbett J. 1984. Monoclonal antibodies protect against respiratory syncytial virus infection in mice. Immunology 52:137–142.

56. Taylor G, Stott EJ, Furze J, Ford J, Sopp P. 1992. Protective epitopes on the fusion protein of respiratory syncytial virus recognized by murine and bovine monoclonal antibodies. J Gen Virol 73:2217–2223. https://doi.org/10.1099/0022-1317-73-9-2217.